Chemical Science

ROYAL SOCIETY OF CHEMISTRY

EDGE ARTICLE

View Article Online
View Journal | View Issue

Cite this: *Chem. Sci.*, 2025, **16**, 20942

All publication charges for this article have been paid for by the Royal Society of Chemistry

Received 22nd July 2025
Accepted 1st October 2025

DOI: 10.1039/d5sc05472a

rsc.li/chemical-science

Ligand-mediated asymmetric dicopper sites for robust catecholase-mimicking catalysis and selective sensing

Bojin Li,[a] Meng Yuan,[a] Nannan Xia,[b] Xun Hu *[a] and Fei He *[a]

Fabricating dicopper centers in nanozymes offers a promising route to mimic catecholase-like catalysis. However, some dicopper centers often suffer from symmetric configurations, which are prone to weakening the O–O bond polarization, thereby limiting O_2 activation. This results in unsatisfactory intrinsic activities of nanozymes, thus hindering their potential sensing applications. Here, we report a catechol oxidase (CO)-like nanozyme (DTD-Cu) engineered with proximal and asymmetrically coordinated dicopper centers *via* a N/S-rich ligand. The unique asymmetric $N_4Cu–CuN_4S$ configuration facilitates the preferential O_2 adsorption/activation and O–O bond polarization as well as the subsequent 4-electron reduction to H_2O *via* a H_2O_2 intermediate, thus endowing DTD-Cu with dramatically enhanced intrinsic activity, as evidenced by orders-of-magnitude improvements in K_m and K_{cat}/K_m over most reported CO-like nanozymes and artificial enzymes. Capitalizing on this superior activity, we achieved highly selective and sensitive detection of the cytotoxic tris(2-carboxyethyl)phosphine (TCEP) with a detection limit of 98.6 ppb *via* a synergistic dual-inhibition mechanism involving both TCEP-induced reduction of the oxidized substrate/ROS and direct TCEP-mediated chelation to the Cu sites.

Introduction

Nanozymes, synthetic mimics of natural enzymes, offer compelling advantages such as high stability, cost-effectiveness, and tunable functionality, holding immense promise in replacing natural enzymes for various applications.[1–7] Among these, catechol oxidase (CO)-like nanozymes, which catalyze the oxidation of catechol derivatives, have recently attracted attention for biomimetic catalysis and analytical sensing.[1,4,5,8] However, a pervasive challenge of existing CO-like nanozymes is their relatively low catalytic activity, often reflected in poor Michaelis constant (K_m) and catalytic efficiency (K_{cat}/K_m) values,[1,9–12] which curtails their potential applications.

To boost the intrinsic activity of CO-like nanozymes, using ligand engineering to control the dicopper site configuration represents one of the effective approaches,[13–16] which could mimic the dicopper centers of natural CO better[17,18] compared with other strategies such as regulating multinuclear metal centers,[1,12] changing the types of metal/support[9] and controlling metal–polymer or supramolecular self-assembly.[5,19] Despite much progress, some artificial dicopper centers often suffer from weak O–O bond polarization due to their symmetric configurations (*i.e.*, $S_1N_3Cu–CuN_3S_1$, $S_1N_2Cu–CuN_2S_1$, $O_1N_3Cu–CuN_3O_1$, and $O_3N_1Cu–CuN_1O_3$),[4,14,15] which limit O_2 activation, thus resulting in unsatisfactory intrinsic activities. In this sense, breaking the symmetric configuration of dicopper sites through ligand engineering may be crucial for boosting the CO-mimicking activity of nanozymes, but it remains a formidable task.

Here, we engineered a CO-like nanozyme (DTD-Cu) featuring proximal and asymmetrically coordinated dicopper catalytic centers by employing 2,5-diamino-1,3,4-thiadiazole (DTD) as a N/S-rich ligand. When applied for CO-mimicking catalysis, the dicopper sites with an asymmetric $N_4Cu–CuN_4S$ configuration promoted O_2 adsorption and activation to generate reactive oxygen species and directed their rapid 4-electron reduction to H_2O, thereby enabling a dramatic enhancement in catalytic kinetic parameters, notably K_m and K_{cat}/K_m, by orders of magnitude compared to previously reported CO-like nanozymes and artificial enzymes. Leveraging this superior activity, as well as the coordination capability of Cu for phosphorus, we demonstrated a highly selective colorimetric sensing platform for trace cytotoxic tris(2-carboxyethyl)phosphine (TCEP), where the detection limit approached 98.6 ppb, lower than that of other sensing systems for detecting P-containing compounds based nanozymes, surface-enhanced Raman spectroscopy (SERS) and fluorescence.

Results and discussion

To construct adjacent dicopper centers, the heterocycle ligand (*i.e.*, 2,5-diamino-1,3,4-thiadiazole, DTD) was chosen due to the

[a]*School of Materials Science and Engineering, University of Jinan, Jinan 250024, China. E-mail: xun.hu@outlook.com; mse_hef@ujn.edu.cn*

[b]*State Key Laboratory of Green Papermaking and Resource Recycling, Key Laboratory of Pulp & Paper Science and Technology of Shandong Province/Ministry of Education, Qilu University of Technology (Shandong Academy of Sciences), Jinan 250353, China*

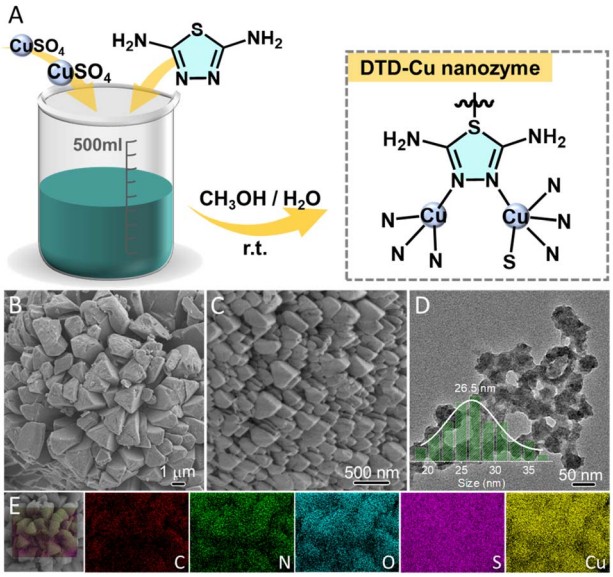

Fig. 1 (A) Schematic illustration of synthesis of the DTD-Cu nanozyme; SEM images of DTD-Cu prepared with (B) and without (C) PVP addition; (D) TEM image of DTD-Cu; (E) EDS mapping of DTD-Cu.

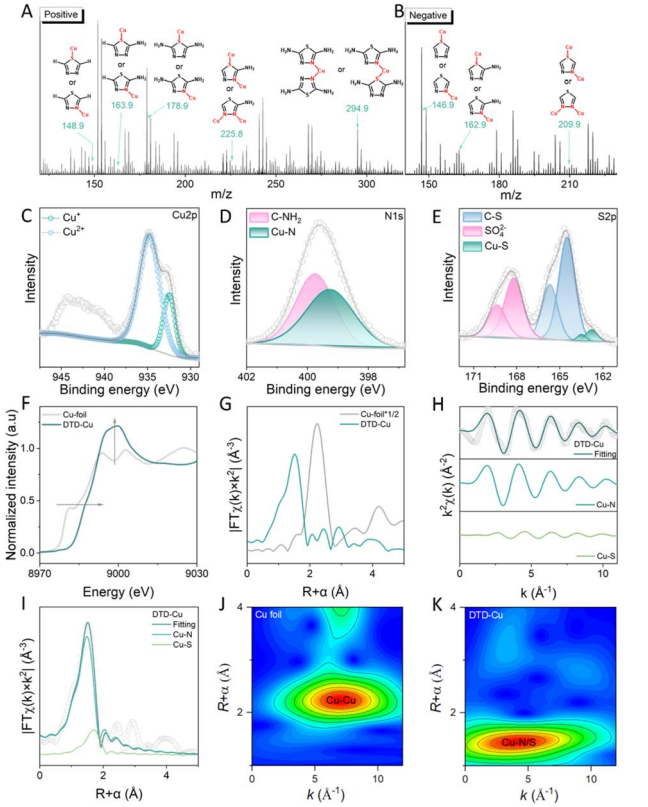

Fig. 2 TOF-SIMS spectra of positive (A) and negative (B) ions and possible assignments; Cu2p (C), N 1s (D) and S 2p (E) XPS spectra of DTD-Cu; (F) Cu K-edge XANES spectra of DTD-Cu and Cu foil; (G) Cu K-edge FT-EXAFS spectra of DTD-Cu and Cu foil in *R* space; (H) Cu K-edge EXAFS fitting analysis of DTD-Cu in *k*-space; (I) FT-EXAFS fitting analysis of DTD-Cu in *R*-space. Cu K-edge WT-EXAFS spectra of Cu foil (J) and DTD-Cu (K).

presence of two neighbouring heterocyclic N atoms, which are capable of coordinating with Cu through a simple one-step complexation (see the Experimental section in the SI). Furthermore, the thiophenic S atom of DTD also possesses coordination potential for Cu, thus contributing to the control of the coordination configuration of the Cu center in DTD-Cu (Fig. 1A).

The microscopic morphology of DTD-Cu was observed using scanning electron microscopy (SEM). DTD-Cu presented as a bulk particle with a size at the micron level (Fig. 1B). When PVP was introduced into the preparation system, the size of DTD-Cu-PVP obviously decreased to the nanometer level compared with that of DTD-Cu (Fig. 1C). The XRD patterns of DTD-Cu and DTD-Cu-PVP were nearly identical (Fig. S1), indicating that adding PVP did not change the structure of DTD-Cu. According to the SEM image, the cross section of the DTD-Cu bulk particle presented an aggregated nanoparticle morphology, which was confirmed by transmission electron microscopy (TEM) (Fig. S2). A similar morphology, accompanied by interconnected nanoparticles with an average size of ~26.5 nm, was also observed for DTD-Cu-PVP (Fig. 1D). Energy dispersive spectroscopy (EDS) mapping showed that the elements C, N, O, S and Cu uniformly distributed in DTD-Cu (Fig. 1E). The Cu content in DTD-Cu was 23.3 wt% based on ICP-OES analysis.

To explore the coordination information of the Cu center, time-of-flight secondary ion mass spectrometry (TOF-SIMS) was carried out to collect the mass fragments ejected from DTD-Cu.[20] The fragment ions with mass to charge ratios (*m*/*z*) of 148.9 ($Cu_1C_2N_2S_1H_2$), 163.9 ($Cu_1C_2N_3S_1H_3$), 178.9 ($Cu_1C_2N_4S_1H_4$) and 294.9 ($Cu_1C_4N_8S_2H_8$) in the positive spectrum as well as 146.9 ($Cu_1C_2N_2S_1$) and 162.9 ($Cu_1C_2N_3S_1H_2$) in the negative spectrum were detected (Fig. 2A and B), which may correspond to Cu_1-coordinated DTD fragments involving Cu–N and/or Cu–S coordination. The possible coordination between the heterocyclic N/S atoms of DTD and Cu was also supported by the appearance of Cu_2-coordinated DTD fragment ions with *m*/*z* of 225.8 ($Cu_2C_2N_3S_1H_2$) and 209.9 ($Cu_2C_2N_2S_1$).

X-ray photoelectron spectroscopy (XPS) was further conducted to determine the Cu–N/S coordination and chemical states of elements in DTD-Cu. According to the XPS survey scan spectrum, C, N, O, S and Cu (Fig. S3) were detected, consistent with the EDS mapping results. In the Cu 2p spectrum, Cu^{2+} and Cu^{+} were observed (Fig. 2C). The N 1s spectrum displayed two signals, which were assigned to Cu–N and C–NH_2 with a ratio of ~1 : 1 (Fig. 2D). This signified that Cu may coordinate with the heterocyclic nitrogen rather than exocyclic –NH_2, similar to the reported results.[14,15] In the S 2p spectrum, we observed three types of S, corresponding to SO_4^{2-}, C–S and Cu–S (Fig. 2E). Fourier-transform infrared (FTIR) spectroscopy also confirmed the existence of SO_4^{2-} (Fig. S4), which may be introduced into DTD-Cu by forming H-bonds with –NH_2 of DTD.[21] Importantly, the appearance of Cu–S implied that apart from two N atoms, the thiophenic S of DTD could also coordinate with the Cu ion. These XPS and TOF-SIMS spectra collectively illustrated that

DTD-Cu contained both the Cu–N and Cu–S coordination centers.

X-ray absorption near-edge structure (XANES) spectroscopy and extended X-ray absorption fine structure (EXAFS) was further analyzed to determine the atomic-scale coordination environment of Cu in DTD-Cu. As shown in Cu K-edge X-ray absorption near-edge structure (XANES) spectra, the edge absorption energy of DTD-Cu was more positive than that of Cu foil (Fig. 2F). Moreover, DTD-Cu also exhibited a higher intensity of the white line peak corresponding to the 1s → $4p_{xy}$ transition compared with Cu foil. These results indicate that the Cu center in DTD-Cu is in an oxidized state.

Fourier-transformed EXAFS spectra (FT-EXAFS) in *R* space showed that DTD-Cu exhibited a characteristic scattering peak at ~1.50 Å, clearly distinct from the Cu–Cu scattering peak at ~2.24 Å (Fig. 2G), suggesting the atomic dispersion of Cu in DTD-Cu. According to the FT-EXAFS signal in *k*-space, we observed two different oscillation periods corresponding to Cu–N and Cu–S paths (Fig. 2H), which favored the formation of Cu–N and Cu–S coordination in DTD-Cu, agreeing with the N 1s/S 2p spectra (Fig. 2D and E). To determine the N/S coordination numbers around the Cu center, fitting analysis of the FT-EXAFS spectrum of DTD-Cu in *R* space was performed. Fig. 2I and Table S1 illustrate that each Cu center was connected with four N atoms, and the average number of coordinating S atoms was 0.5 in DTD-Cu, which indicated that only one Cu atom of the adjacent dicopper centers coordinated with the thiophenic S atom of DTD, thus generating the asymmetric $N_4Cu–CuN_4S$ configuration at the adjacent dicopper centers. In addition, the intensity maximum of wavelet-transformed (WT)-EXAFS spectra of DTD-Cu was situated at ~1.46 Å, clearly different from that of Cu foil (2.23 Å). This verified the atomic dispersion of Cu in DTD-Cu, consistent with FT-EXAFS. All of these results illustrate that the N/S-rich DTD ligand preferentially coordinates with Cu through the Cu–N and Cu–S bonds, thereby generating the asymmetric $N_4Cu–CuN_4S$ configuration at the adjacent binuclear Cu centers of DTD-Cu.

Using 3,5-ditert-butyl catechol (3,5-DTBC) as a model molecule, we evaluated the catechol oxidase-like catalytic activity of DTD-Cu. As depicted in Fig. 3A, the characteristic absorbance of 3,5-DTBC in the air-saturated blank solution appeared at 280 nm. After DTD-Cu was mixed with 3,5-DTBC in the catalytic system, the colorless solution gradually became yellow and a new peak at 416 nm emerged, which was assigned to the product 3,5-di-*tert*-butyl-benzoquinone (3,5-DTBQ). This demonstrated the catechol oxidase-like activity of DTD-Cu. Moreover, increasing the O_2 concentration of the catalytic system led to an obvious enhancement in the catalytic activity of DTD-Cu, suggesting that DTD-Cu was capable of activating O_2 to oxidize 3,5-DTBC. Once DTD-Cu was filtered using a filter membrane with average pore size of 100 nm, the reaction rate obviously decreased (Fig. S5). When the pH of the buffer solution varied from 3 to 8, DTD-Cu presented enhanced catalytic activity (Fig. S6). In order to compare with the reported catechol oxidase-like artificial enzymes,[1,4] a buffer solution with pH 8 was chosen to assess the catalytic activity of DTD-Cu. Meanwhile,

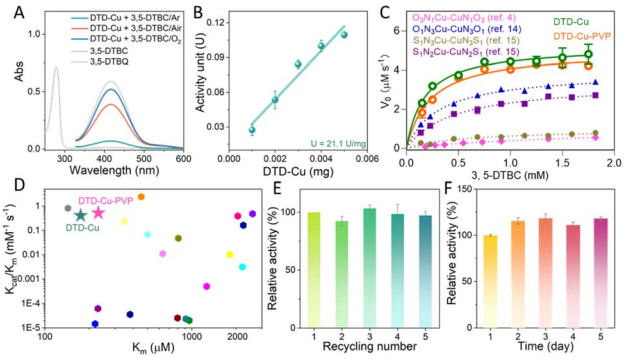

Fig. 3 (A) UV-vis spectra of 3,5-DTBC, 3,5-DTBQ and 3,5-DTBC in air-, O_2- and N_2-saturated PBS (pH = 8)/CH_3CN solution with DTD-Cu; (B) specific activity of DTD-Cu; (C) Michaelis–Menten curves of DTD-Cu and recently reported nanozymes; (D) comparison of kinetic parameters (K_m and K_{cat}/K_m) among DTD-Cu, recently reported artificial molecular enzymes and nanozymes; (E) relative activities of DTD-Cu during the recycling process; (F) storage stability of DTD-Cu in air at room temperature.

the catalytic activity of DTD-Cu did not notably decrease after adding K^+, Na^+ and Cl^- into the catalytic system (Fig. S7).

According to Fig. 3B, the specific activity of DTD-Cu approached 21.1 U mg^{-1}. Moreover, DTD-Cu-PVP with its smaller size showed a higher specific activity, which reached 38.6 U mg^{-1} (Fig. S8), superior to that of many reported catechol oxidase-like artificial enzymes (Table S2).[13–15] Meanwhile, the intrinsic activity of DTD-Cu was further evaluated by varying the concentration of 3,5-DTBC. The catalytic reaction rate shown by DTD-Cu followed Michaelis–Menten kinetics (Fig. 3C) and surpassed that of reported nanozymes with symmetric dicopper site configurations (*i.e.*, $S_1N_3Cu–CuN_3S_1$, $S_1N_2Cu–CuN_2S_1$, $O_1N_3Cu–CuN_3O_1$, and $O_3N_1Cu–CuN_1O_3$).[4,14,15] Based on the Michaelis–Menten equation, the kinetic parameters including K_m, K_{cat} and K_{cat}/K_m were further acquired by non-linear curve fitting analysis. As seen in Fig. 3D and Table S3, the K_m and K_{cat}/K_m values of DTD-Cu exceeded those of most catechol oxidase-like artificial enzymes and nanozymes,[1,4,5,12,14,15,19,22] demonstrating the superior catalytic activity of DTD-Cu. The relative activity of DTD-Cu did not decrease after five recycling cycles (Fig. 3E). Even after being stored in water for 5 days, DTD-Cu did not show significant decay in catalytic activity (Fig. 3F). These activity assessments demonstrate the superior catalytic capability of DTD-Cu, indicating its potential as a new artificial enzyme for catalytic colorimetric detection.

To further understand the catalytic mechanism of DTD-Cu, electrochemical characterization, EPR testing and specific capture experiments were performed. In an Ar-saturated solution at pH 8, the redox transition peak of Cu^{2+}/Cu^+ was observed in the cyclic voltammetry (CV) curve of DTD-Cu. After this solution was saturated with O_2, a strong reduction current was observed (Fig. 4A), indicating the obvious oxygen reduction activity of DTD-Cu. Importantly, we also observed obvious redox peaks in the CV curves (Fig. 4B) when DTD-Cu catalyzed the 3,5-DTBC oxidation reaction. However, once Ar was replaced with O_2, these redox peaks shifted negatively. This may be because

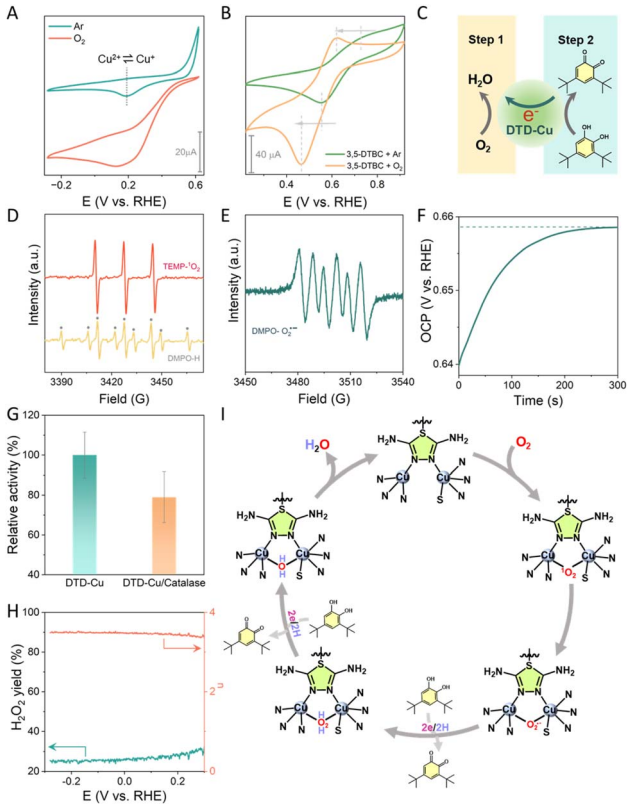

Fig. 4 (A) CV curves of DTD-Cu in the presence of Ar or O_2; (B) CV curves of DTD-Cu in the presence of 3,5-DTBC under Ar or O_2; (C) schematic illustration of electron transfer during the 3,5-DTBC oxidation and O_2 reduction processes; ESR spectra recorded for trapping $^1O_2$/$^{\bullet}$OH (D) and $O_2^{\bullet-}$ (E); (F) OCP curve over time; (G) specifically trapping H_2O_2 during DTD-Cu-catalyzed oxidation of 3,5-DTBC using catalase; (H) electron transfer number (*n*) and H_2O_2 yield of DTD-Cu during electrocatalytic oxygen reduction; (I) proposed mechanism of CO-like catalysis at dicopper sites of DTD-Cu.

O_2 is preferentially adsorbed and activated at the binuclear Cu sites of DTD-Cu during catalysis compared with 3,5-DTBC (Fig. 4C), which leads to an elevated electrochemical potential, facilitating the oxidation of 3,5-DTBC. The collected electron spin resonance (ESR) spectra supported this deduction, showing that the obvious $^1O_2$ signal was detected for DTD-Cu only in the presence of air and TEMP without adding 3,5-DBTC (Fig. 4D). Due to the asymmetric configuration of di-copper centers, the O–O bond in the formed $^1O_2$ could be further polarized by acquiring electrons from the Cu site to produce $O_2^{\bullet-}$ only in the presence of air and DMPO without adding 3,5-DBTC (Fig. 4E).

Once the Cu sites transferred electrons to polarize the adsorbed O_2 to form $O_2^{\bullet-}$, DTD-Cu became more electron-deficient, thus elevating the electrochemical potential of DTD-Cu to drive the 3,5-DBTC oxidation. Meanwhile, this increased electrochemical potential reduced the reducing capability of DTD-Cu, which would attenuate the rate of oxygen reduction reaction (ORR). Accordingly, the "mixed potential" (*i.e.*, open-circuit potential (OCP)) of the reductive and oxidative half-reactions[14,23] continuously changed until the rates of ORR and 3,5-DBTC oxidation were balanced to attain a steady state, as supported by the collected OCP curve (Fig. 4F). These results confirm that the preferential adsorption and activation of O_2 is the crucial initial step in mimicking CO-like catalysis, and that the asymmetric dicopper centers of DTD-Cu subsequently polarize the O–O bond to generate $O_2^{\bullet-}$ by transferring electrons.

The formed $O_2^{\bullet-}$ further acquired electrons and protons to produce H_2O_2, as demonstrated by the catalase trapping experiment (Fig. 4G). This H_2O_2 intermediate was also detected by the rotating ring-disc electrode (RRDE) test (Fig. 4H). Given that the ORR driven by DTD-Cu is a 4e-dominated process (Fig. 4H), the produced H_2O_2 could be further reduced to form H_2O by accepting electrons and protons, accompanied by the oxidation of 3,5-DTBC. Interestingly, the $^{\bullet}$OH signal was not detected during catalysis. Thus, the possible catalytic mechanism driven by DTD-Cu was proposed (Fig. 4I). After O_2 is preferentially adsorbed at the Cu site of DTD-Cu, it undergoes a continuous 4e transformation process, $^3O_2 \rightarrow {}^1O_2 \rightarrow O_2^{\bullet-} \rightarrow H_2O_2 \rightarrow H_2O$, accompanied by the oxidation of 3,5-DTBC.

Based on this catalytic colorimetric system enabled by the outstanding CO-like catalytic activity of DTD-Cu, we detected organophosphorus compounds that are commonly used in flame retardants, pesticides and insecticides.[24,25] We chose cytotoxic tris(2-carboxyethyl)phosphine (TCEP) as a model P-based compound.[26] TCEP was directly mixed with the reaction solution containing DTD-Cu and 3,5-DTBC. After 3 min, the solution was monitored using UV-vis spectroscopy. Compared with the control group, the absorbance of the solution decreased significantly once 1.75 ppm TCEP was introduced (Fig. 5A), indicating that this catalytic colorimetric system driven by DTD-Cu is suitable for detecting TCEP. By varying the concentration of TCEP in the catalytic system, the limit of detection (LOD) was determined to be 98.6 ppb (Fig. 5B), which is comparable to that of other sensing systems for detecting organophosphorus compounds based on nanozymes, surface-enhanced Raman spectroscopy (SERS) and fluorescence (Table S4).[27–29] Furthermore, the LOD for sensing TCEP in this DTD-Cu system was also lower than that of HPLC-ELSD and other nanozyme catalytic systems (Table S4). Importantly, apart from TCEP, various inorganic ions (K^+, Na^+, Cl^-, NO_3^-, and SO_4^{2-}), glucose (Glu) and phosphate ester flame retardants such as triethyl phosphate (TEP), triphenyl phosphate (TPP), tributyl phosphate (TBP), tris(2-chloroethyl) phosphate (TClEP) and tris(1-chloro-2-propyl) phosphate (TClPP) did not show any notable inhibition effect on the DTD-Cu-driven catalytic colorimetric system (Fig. 5C and D). According the reported results,[30] the molecular volumes of TPP and TCEP were similar, indicating their similar steric effects. However, the inhibitory effect of TPP on the catalytic activity of DTD-Cu was much weaker (Fig. 5D). This result indicated that the steric effect is not the main reason for the selective sensing behavior of DTD-Cu toward these organophosphorus compounds. Likewise, the catalytic activity of DTD-Cu did not present a notable decrease after adding the reducing agent epinephrine into this catalytic system, which is different from the effect observed with TCEP

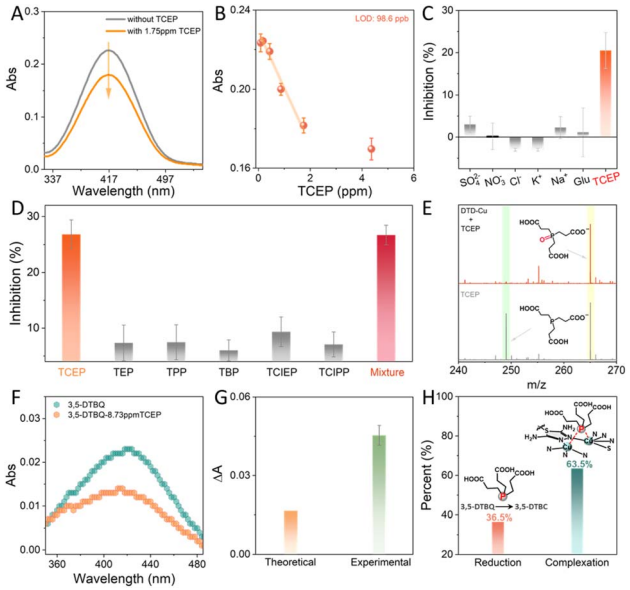

Fig. 5 (A) UV-vis spectra monitoring the DTD-Cu-catalyzed 3,5-DTBC oxidation in the absence and presence of TCEP; (B) linear plot of absorbance (416 nm) *versus* the concentration of TCEP in the DTD-Cu-driven colorimetric system; selectivity of DTD-Cu for detecting TCEP in the presence of various interfering ions (C) and organophosphorus molecules (D); (E) high-resolution mass spectrometry of reaction solution involving DTD-Cu and TCEP; (F) UV-vis spectra of 3,5-DTBQ in the absence and presence of TCEP; (G) comparison of theoretical and experimental absorbance of systems in the presence of 1.75 ppm TCEP; (H) contribution of reduction and complexation by TCEP to the inhibition of the catalytic colorimetric process of DTD-Cu.

(Fig. S9). This indicates that TCEP could be selectively detected using this DTD-Cu-driven catalytic system.

Given that DTD-Cu activates O_2 to generate ROS during catalysis and that TCEP is capable of quenching ROS, we speculated that TCEP may inhibit the catalytic colorimetric process by quenching ROS. If this hypothesis is correct, the oxidation product of TCEP could be detected. To verify the above hypothesis, high-resolution mass spectrometry (HRMS) was conducted to analyze the reaction solution containing DTD-Cu and TCEP. The oxidation product tris(carboxyethyl)phosphine oxide (TCEPO) was detected, and TCEP almost disappeared after 3 min (Fig. 5E). This result indicates that ROS may be quenched by the electron-rich P of TCEP through a reduction reaction. Moreover, individually adding TCEP to a yellow 3,5-DTBQ solution without DTD-Cu led to a significant decrease in the absorbance of solution(Fig. 5F), which was because TCEP is also capable of reducing 3,5-DTBQ.[31]

Both quenching of ROS and reduction of 3,5-DTBQ would essentially cause the oxidation of TCEP to form TCEPO, accompanied by a 2e transfer. Consuming one TCEP molecule is equivalent to eliminating one 3,5-DTBQ molecule. If we assume that TCEP inhibited the catalytic colorimetric process only by quenching ROS and reducing 3,5-DTBQ, the absorbance change of the solution was theoretically calculated based on the linear working curve of 3,5-DTBQ. According to this assumption, the theoretical absorbance change of solution should be 0.017 upon adding 1.75 ppm TCEP (Fig. 5G). However, the experimental results showed that the absorbance change of solution was 0.045, significantly exceeding the theoretical value. This result, together with the coordination potential of the electron-rich P in TCEP, illustrates that in addition to quenching ROS and reducing 3,5-DTBQ, TCEP is capable of competing with O_2 for the Cu sites of DTD-Cu *via* the complexation effect to inhibit the catalytic colorimetric process.[32] Accordingly, we calculated that the inhibition originating from the complexation effect and reduction potential of TCEP accounted for 63.5% and 36.5%, respectively (Fig. 5H), which suggested that the contribution of the complexation effect to the inhibition of the catalytic colorimetric process is dominant compared with that of quenching ROS and 3,5-DTBQ reduction, thereby enabling the selective detection of TCEP using this DTD-Cu-driven catalytic colorimetric system.

Conclusions

In summary, we have addressed the challenge of low intrinsic activity in CO-mimicking nanozymes by designing proximal and asymmetrically coordinated dicopper catalytic centers in DTD-Cu. This unique ligand-mediated asymmetric $N_4Cu–CuN_4S$ configuration enabled a dramatic enhancement in CO-like catalytic efficiency by orders of magnitude compared to previously reported nanozymes and artificial enzymes. Leveraging this exceptional catalytic performance as well as the high affinity of Cu for phosphorus, we developed a highly selective and sensitive colorimetric sensing platform for TCEP, achieving a detection limit of 98.6 ppb. This outstanding sensing capability is attributed to a synergistic dual-inhibition mechanism involving both TCEP-induced reduction of the oxidized substrate and direct TCEP chelation to the copper active sites, with the latter playing a dominant role in achieving high selectivity. This work not only presents a breakthrough in designing highly active biomimetic dicopper nanozymes by precisely tuning ligand-mediated asymmetry but also offers a powerful platform for catalytic sensing, opening new avenues for advanced catalyst design.

Author contributions

F. H. conceived and designed the experiments. B. L. performed the synthesis and/or activity evaluation of the nanozyme. N. X. provided help in applying for the funding. F. H. wrote and revised the manuscript. F. H. and X. H. supervised the project.

Conflicts of interest

The authors declare no competing financial interests.

Data availability

The data that support the findings of this study are available in the supporting information (SI). Supplementary information is available. See DOI: **https://doi.org/10.1039/d5sc05472a**.

Acknowledgements

This work was financially supported by the National Natural Science Foundation of China (No. 52276195), the Doctoral Fund Project of University of Jinan (XBS2409), the Opening Project of State Key Laboratory Incubation Base for Green Processing of Chemical Engineering (Shihezi University, China), the Foundation (No. GZKF202335) of the State Key Laboratory of Biobased Material and Green Papermaking (Qilu University of Technology, Shandong Academy of Sciences), the Program for Supporting Innovative Research from Jinan (202228072) and the Program of Agricultural Development from Shandong (SD2019NJ015). The authors extend their gratitude to Mr Yanda Du from Shiyanjia Lab (**https://www.shiyanjia.com**) for providing invaluable assistance with the XPS analysis.

Notes and references

1 M. Li, J. Chen, W. Wu, Y. Fang and S. Dong, *J. Am. Chem. Soc.*, 2020, **142**, 15569–15574.
2 S. Ji, B. Jiang, H. Hao, Y. Chen, J. Dong, Y. Mao, Z. Zhang, R. Gao, W. Chen and R. Zhang, *Nat. Catal.*, 2021, **4**, 407–417.
3 P. Makam, S. S. Yamijala, V. S. Bhadram, L. J. Shimon, B. M. Wong and E. Gazit, *Nat. Commun.*, 2022, **13**, 1505.
4 M. Sha, L. Rao, W. Xu, Y. Qin, R. Su, Y. Wu, Q. Fang, H. Wang, X. Cui and L. Zheng, *Nano Lett.*, 2023, **23**, 701–709.
5 S. Xu, H. Wu, S. Liu, P. Du, H. Wang, H. Yang, W. Xu, S. Chen, L. Song and J. Li, *Nat. Commun.*, 2023, **14**, 4040.
6 Y. Xu, J. Xue, Q. Zhou, Y. Zheng, X. Chen, S. Liu, Y. Shen and Y. Zhang, *Angew. Chem., Int. Ed.*, 2020, **59**, 14498–14503.
7 G. Li, H. Liu, T. Hu, F. Pu, J. Ren and X. Qu, *J. Am. Chem. Soc.*, 2023, **145**, 16835–16842.
8 J. Wang, R. Huang, W. Qi, R. Su, B. P. Binks and Z. He, *Appl. Catal., B*, 2019, **254**, 452–462.
9 Y. Lin, F. Wang, J. Yu, X. Zhang and G.-P. Lu, *J. Hazard. Mater.*, 2022, **425**, 127763.
10 W. Zou, Y. Liu, R. Li and R. Guo, *ACS Sustain. Chem. Eng.*, 2022, **10**, 10057–10067.
11 D. Kim, G. Gwak, J. Han, D. Kim and O. S. Jung, *Dalton Trans.*, 2022, **51**, 5810–5817.
12 J. Wang, R. Huang, W. Qi, R. Su and Z. He, *Chem. Eng. J.*, 2022, **434**, 134677.
13 M. Yuan, K. Han, H. Yang, L. Mi, C. Huang, X. Hu and F. He, *Small*, 2024, e2401756.
14 M. Yuan, N. Xia, X. Hu and F. He, *Small*, 2024, **20**, e2403850.
15 M. Yuan, N. Xia, Z. Huang, C. Huang, X. Hu and F. He, *Chem. Sci.*, 2024, **15**, 19513–19519.
16 R. V. Morajkar, A. P. Fatrekar and A. A. Vernekar, *Chem. Sci.*, 2024, **15**, 10810–10822.
17 T. Klabunde, C. Eicken, J. C. Sacchettini and B. Krebs, *Nat. Struct. Biol.*, 1998, **5**, 1084–1090.
18 C. Gerdemann, C. Eicken and B. Krebs, *Acc. Chem. Res.*, 2002, **35**, 183–191.
19 S. Thanneeru, N. Milazzo, A. Lopes, Z. Wei, A. M. Angeles-Boza and J. He, *J. Am. Chem. Soc.*, 2019, **141**, 4252–4256.
20 Y. X. Zhang, S. Zhang, H. Huang, X. Liu, B. Li, Y. Lee, X. Wang, Y. Bai, M. Sun, Y. Wu, S. Gong, X. Liu, Z. Zhuang, T. Tan and Z. Niu, *J. Am. Chem. Soc.*, 2023, **145**, 4819–4827.
21 E. Aznar, S. Ferrer, J. Borrás, F. Lloret, M. Liu-González, H. Rodríguez-Prieto and S. García-Granda, *Eur. J. Inorg. Chem.*, 2006, **2006**, 5115–5125.
22 S. Liu, Y. He, W. Zhang, T. Fu, L. Wang, Y. Zhang, Y. Xu, H. Sun and H. Zhao, *Small*, 2024, **20**, e2306522.
23 W. C. Howland, J. B. Gerken, S. S. Stahl and Y. Surendranath, *J. Am. Chem. Soc.*, 2022, **144**, 11253–11262.
24 X. Wang, S. Dong, Q. Zhu, X. Wu, W. Zhou, C. Liao and G. Jiang, *Environ. Sci. Technol.*, 2024, **58**, 14786–14796.
25 B. Shen, Q. Wu, Y. Guo, J. Qin, H. Chen, Y. Yang, Z. Liu, L. Li, W. Li and C. Zhu, *Adv. Funct. Mater.*, 2024, **35**, 2415854.
26 I. Koh, I. Yong, B. Kim, D. Choi, J. Hong, Y. M. Han and P. Kim, *ACS Biomater. Sci. Eng.*, 2020, **6**, 813–821.
27 X. Yan, H. Li, Y. Yan and X. Su, *Food Chem.*, 2015, **173**, 179–184.
28 J. Sun, L. Gong, Y. Lu, D. Wang, Z. Gong and M. Fan, *Analyst*, 2018, **143**, 2689–2695.
29 P. Weerathunge, B. K. Behera, S. Zihara, M. Singh, S. N. Prasad, S. Hashmi, P. R. D. Mariathomas, V. Bansal and R. Ramanathan, *Anal. Chim. Acta*, 2019, **1083**, 157–165.
30 B. Li, N. Xia, C. Huang, X. Hu and F. He, *Chem. Sci.*, 2025, **16**, 14793–14799.
31 B. C. Martindale, E. Joliat, C. Bachmann, R. Alberto and E. Reisner, *Angew. Chem., Int. Ed.*, 2016, **55**, 9402–9406.
32 P. Mei, Z. Ma, Y. Chen, Y. Wu, W. Hao, Q.-H. Fan and W.-X. Zhang, *Chem. Soc. Rev.*, 2024, **53**, 6735–6778.